

Nature of Reactive Hydrogen for Ammonia Synthesis over a Ru/C12A7 Electride Catalyst

James Kammert,[#] Jisue Moon,[#] Yongqiang Cheng, Luke Daemen, Stephan Irle, Victor Fung, Jue Liu, Katharine Page, Xiaohan Ma, Vincent Phaneuf, Jianhua Tong, Anibal J. Ramirez-Cuesta, and Zili Wu*

Cite This: *J. Am. Chem. Soc.* 2020, 142, 7655–7667

Read Online

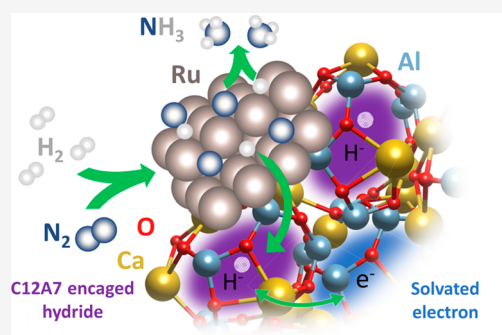
ACCESS |

Metrics & More

Article Recommendations

Supporting Information

ABSTRACT: Recently, there have been renewed interests in exploring new catalysts for ammonia synthesis under mild conditions. Electride-based catalysts are among the emerging ones. Ruthenium particles supported on an electride composed of a mixture of calcium and aluminum oxides (C12A7) have attracted great attention for ammonia synthesis due to their facile ability in activating N₂ under ambient pressure. However, the exact nature of the reactive hydrogen species and the role of electride support still remain elusive for this catalytic system. In this work, we report for the first time that the surface-adsorbed hydrogen, rather than the hydride encaged in the C12A7 electride, plays a major role in ammonia synthesis over the Ru/C12A7 electride catalyst with the aid of *in situ* neutron scattering techniques. Combining *in situ* neutron diffraction, inelastic neutron spectroscopy, density functional theory (DFT) calculation, and temperature-programmed reactions, the results provide direct evidence for not only the presence of encaged hydrides during ammonia synthesis but also the strong thermal and chemical stability of the hydride species in the Ru/C12A7 electride. Steady state isotopic transient kinetic analysis (SSITKA) of ammonia synthesis showed that the coverage of reactive intermediates increased significantly when the Ru particles were promoted by the electride form (coverage up to 84%) of the C12A7 support rather than the oxide form (coverage up to 15%). Such a drastic change in the intermediate coverage on the Ru surface is attributed to the positive role of electride support where the H₂ poisoning effect is absent during ammonia synthesis over Ru. The finding of this work has significant implications for understanding catalysis by electride-based materials for ammonia synthesis and hydrogenation reactions in general.



1. INTRODUCTION

Synthesis of ammonia via the Haber–Bosch process has played an increasingly critical role in global food production since its inception in the early 20th century.¹ As a result, approximately 50% of the world population depends on artificially fixed nitrogen for sustenance, and some predictions of future demand for reactive nitrogen suggest that soon a majority of the world will depend on artificial nitrogen fixation not only for their food resources but also potentially for the production of ammonia for fuels, hydrogen storage, and biomass-derived chemicals.^{2–4} Prevailing ammonia synthesis catalysts are Fe-based and demonstrate strong structure sensitivity in the ammonia synthesis reaction.⁵ Seven-coordinate Fe sites (C7 sites), such as those located on Fe(111) surfaces, are believed to be the active sites for rate-limiting N₂ dissociation.^{6–8} Iron-based catalyst systems, however, demonstrate low activity for ammonia synthesis, requiring temperatures between 673 and 773 K to obtain appreciable formation rates of ammonia. At such temperatures, ammonia synthesis equilibrium strongly favors the reactants H₂ and N₂, and the reaction must be carried out under extreme pressure (15–30 MPa) to obtain economical yields of ammonia.

Basic-metal-promoted Ru supported on carbon catalyzes ammonia synthesis at lower temperatures than conventional Fe catalysts, and these Ru nanoparticle catalysts have received extensive attention as ammonia synthesis catalysts, as summarized in a recent review by Saadatjou et al.⁹ The role of the alkali promoters in supported Ru catalysts has also received significant research attention, and a summary of some of the key findings of recent research can be found in a review by K. Aika.¹⁰ These Ru catalysts are also structure sensitive, favoring specific types of step sites on the Ru surface (B5 sites).^{11–15} They suffer, however, from a H₂ poisoning effect, which manifests as a negative reaction order in H₂, limiting catalyst performance at high pressure. This effect is believed to arise from the out-competition of N₂ adsorption by H₂ adsorption on the Ru catalyst surface.^{9,10,14} Blocking N₂

Received: February 28, 2020

Published: April 4, 2020



adsorption sites with adsorbed H is expected to significantly affect ammonia synthesis rates over Ru catalysts because N_2 dissociation is also expected to be the rate-limiting step in the Ru system, even when promoted by basic metals.^{15,16}

Advances in materials synthesis enabled the formation of ionic crystals containing solvated electrons, known as electrides, in systems that are stable under atmospheric conditions. One example of such a material is a mixture of calcium and aluminum oxides (structure $[Ca_{24}Al_{28}O_{64}]^{4+}$ ($4e^-$), abbreviated C12A7: e^-), which, after high-temperature treatment, can form a stable crystal structure containing solvated electrons where framework oxygens have been displaced.¹⁷ The electride's unique crystal structure consists of a positively charged framework with the chemical formula $[Ca_{24}Al_{28}O_{64}]^{4+}$ that is organized into a repeating network of cages ~ 4.8 Å in diameter that may contain a variety of anions including oxygen, hydride, or nitride species. In the absence of an adequately charged anion (i.e., the electride form), empty cages may also stabilize solvated electrons having an unusually low work function. When C12A7: e^- is used as a support for Ru particles, an ammonia synthesis catalyst is formed that demonstrates remarkably high activity.^{18–20} The presence of electrons with low work function in the support framework was proposed to be responsible for the comparably higher activity, as has been seen in several electride-supported Ru systems or systems including Ru, Fe, or Co on electride-like supports, such as perovskite oxyhydrides like $BaTiO_3$.^{18,21–25} Promise has also been seen in alkali and alkaline earth hydride-based catalysts, which were recently reported.^{26–29} Recent work studying Ca_2N , however, suggests the rate is enhanced even when the electride is converted completely to the hydride Ca_2NH structure.²⁴

While it is clear that electron-rich or defected supports containing electrons with low work functions promote catalytic ammonia synthesis, the mechanism of this promotional effect remains unclear. The presence of electrons with low work functions is proposed to promote ammonia synthesis in a similar manner to the promotion of Ru by basic metals, by donating electron density into N_2 species adsorbed on the Ru surface, thus weakening the $N\equiv N$ bond. The promoting role of support hydride species in the formation of ammonia has also been proposed.^{18–20,24} So-called “nascent” hydride species formed by the electride were proposed to play a key role in ammonia synthesis. Observed kinetic behavior, however, in the Ru/electride systems suggests ammonia synthesis is catalyzed in a regime where N_2 dissociation is no longer the rate-determining step³⁰ as H_2 poisoning of the ammonia synthesis reaction is no longer evident when the reaction is carried out in the presence of the electride and hydride materials. This lack of H_2 poisoning was attributed to the ability of the support material to reversibly store hydride species, which unfortunately has no direct experimental evidence.

In this work, we aim to characterize the hydride species in the C12A7: e^- electride during ammonia synthesis and provide insight into the significance of these species in catalyzing ammonia synthesis over electride materials. Neutron scattering techniques used here including neutron diffraction and inelastic neutron scattering offer the opportunity to directly observe H-containing species in the C12A7: e^- lattice and determine how they evolve under various treatments, and density functional theory (DFT) calculations are used for the interpretation of neutron scattering data and the study of hydrogen migration through the electride. Additionally,

observations from kinetic studies including steady-state isotopic transient kinetic analysis (SSITKA) are used to support a hypothesis for why H_2 poisoning is mitigated in the presence of the electride-supported Ru catalysts.

2. MATERIALS AND METHODS

The $12CaO\cdot 7Al_2O_3$ (C12A7) oxide ($C12A7:O^{2-}$) powders were synthesized by a modified Pechini method.³¹ Briefly, a stoichiometric amount of $Ca(NO_3)_2\cdot 4H_2O$ and $Al(NO_3)_3\cdot 9H_2O$ was dispersed into an aqueous solution of EDTA and citric acid by continuous stirring at room temperature. The molar ratio of EDTA, citric acid, and metal ions is 1.5:1.5:1. After that, the ammonium hydroxide ($NH_3\cdot H_2O$) solution was slowly added in the above slurry until the formation of a clear solution. The pH of this solution is around 10. After the evaporation of water, a claybank gel was obtained, which was then dried in an oven at 150 °C for 48 h to get the charcoal-like powders. Pure mayenite (C12A7) was obtained by calcining the charcoal-like primary powders in air at 1473 K for 10 h with a ramp of 5 K min^{-1} . The $12CaO\cdot 7Al_2O_3$ electride ($C12A7:e^-$) powders were synthesized via a one-step aluminothermic method directly from a mixture of commercially available CaO, Al_2O_3 , and Al powders.³² Calcium oxide (CaO, reagent grade), calcium carbonate ($CaCO_3$, 99.5%), and gamma phase aluminum oxide ($\gamma-Al_2O_3$, 99.9%) are used as received from Alfa-Aesar. Aluminum (Al, reagent grade) powders are obtained from Fisher Scientific. Briefly, the CaO, Al_2O_3 , and Al powders with molar ratios of 12:6.3:0.14 were manually mixed in an agate mortar. Afterward, the well-mixed powder precursor was placed in an alumina crucible with an alumina plate cover, which was then calcined in a horizontal tube furnace at 1473 K for 8 h in a flowing Ar atmosphere. After cooling in the same inert atmosphere, C12A7: e^- powders with a pure mayenite structure were obtained. The Ru was added to the C12A7 supports using a vapor deposition method as outlined by Kitano et al.¹⁸ Analysis of the Ru loading on each sample was carried out using inductively coupled plasma optical emission spectroscopy by Galbraith Laboratories in Knoxville, TN.

Adsorption of CO was performed using a Micromeritics 3Flex instrument, to estimate the number of exposed Ru atoms in each catalyst sample. Dihydrogen chemisorption was not used to avoid uptake of H by the electride cages. Each sample was pretreated by dosing the sample with 67 kPa H_2 at 323 K for 1 h and subsequently evacuated at the same temperature for 1 h. The sample was then heated to 673 K where it was dosed again with 67 kPa H_2 for 1 h and again evacuated at the same temperature for 1 h. Dosing and evacuation cycles at 673 K were repeated three times. The adsorbent CO (99.9%, Airgas) was then dosed onto the catalyst surface at 308 K from 0 to 67 kPa. The total chemisorption of CO was determined by extrapolating the total uptake in the linear region of the isotherm from high pressure to zero pressure. This quantity was then used to determine the dispersion of the Ru surface. While CO chemisorption has been seen at ratios ranging from 0.2 to 1.5, a stoichiometry of 1:1 for $CO_{ads}:Ru_{surface}$ has been assumed herein.³³

Diffraction studies were carried out using both X-ray and neutron diffraction. X-ray diffraction (XRD) experiments were performed using a PANalytical X'Pert Pro MPD diffractometer with $Cu-K\alpha$ radiation ($\lambda = 1.5418$ Å). The step size for each measurement was 0.0167. *In situ* neutron diffraction studies were carried out at beamline BL-1B (NOMAD) at the Spallation Neutron Source (SNS) at Oak Ridge National Laboratory (ORNL). Powder samples were pressed into pellets at 5 t and then crushed and sieved to size between 100 and 500 μm . Samples were loaded individually into a quartz glass tube sealed with a plug valve at room temperature on NOMAD.³⁴ Before measurement, the sample was purged with He (15 $cm^3 min^{-1}$) at room temperature for 2 h to purge the connected gas line. Afterward, the temperature was increased to 673 K and held for 30 min to remove any water retained by the sample. After pretreatment, the gas was switched to an ambient-pressure gas mixture of D_2 and N_2 (3:1 $D_2:N_2$, total flow rate 40 $cm^3 min^{-1}$) for 4 h at the same temperature (673 K). Diffraction patterns were then collected every 10 min. Subsequently, the N_2 gas was switched off, and the sample was treated

with pure D₂ (30 cm³ min⁻¹) for 2 h followed by treatment in pure N₂ (30 cm³ min⁻¹) for 3 h. After N₂ treatment, the sample was exposed to the original 3:1 D₂:N₂ gas mixture again.

Rietveld refinement of the crystal structures obtained from powder neutron diffraction was performed using the program GSAS-II.³⁵ The zero point of the scale, three reflection widths (Caglioti formula, *U*, *V*, and *W*), the lattice parameter, the atomic site parameter, and the isotropic thermal displacement parameters were allowed to vary during refinements. A Fourier difference map was used to identify changes in the crystal structure of the electride cage. The pristine structure of the mayenite electride was used as the starting model for the refinement in GSAS-II. After converging, the Fourier difference map was calculated and plotted using VESTA software³⁶ with a positive residual threshold value of 0.3 fm/Å.

The inelastic neutron scattering (INS) spectra were measured at beamline BL-16B (VISION) at the SNS at ORNL. The sample (about 12 g of 2 wt % Ru/C12A7:e⁻) was loaded into a stainless-steel container for analysis. The sample container was attached to a gas handling sample stick, which was used to perform gas-phase pretreatment and reactions. The sample in the reaction container was first evacuated at room temperature and then cooled to the base temperature (5 K) for background measurement. After background measurement, the sample container was first heated to 673 K, filled to 1 bar with a 3:1 H₂:N₂ gas mixture, and held for 2 h. The sample was then evacuated, and the 2 h treatment in 3:1 H₂:N₂ was repeated (step 1). Next, the sample was treated under a vacuum for 4 h (step 2). After vacuum treatment, the sample was heated to 873 K, and steps 1 and 2 were repeated. The sample was then treated under 0.1 MPa pure H₂ gas for 4 h (step 3). After hydrogen treatment, the container was filled with 0.1 MPa N₂ gas, held for 20 min, and evacuated. This cycle was repeated 5 times (step 4). After each numbered step, the sample was cooled to 393 K and evacuated to remove unreacted gas and then cooled to 5 K to collect an INS spectrum. Steps 3 and 4 at 673 K were conducted as a separate experiment using 6 g of fresh sample, after measurement of the new background over the new sample.

Density functional theory (DFT) calculations were performed using the Vienna ab initio simulation package (VASP).³⁷ The generalized gradient approximation (GGA) was employed in conjunction with the exchange-correlation functional of Perdew, Burke, and Ernzerhof (PBE).³⁸ The projector-augmented wave (PAW) method³⁹ was used to couple ultrasoft pseudopotentials⁴⁰ to the augmented plane-wave basis with a cutoff energy of 400 eV. Convergence of the wave function was determined using an energy threshold of 10⁻⁶ eV. The C12A7:e⁻ electride was modeled using a neutral cubic unit cell containing two molecules of the 12CaO·7Al₂O₃ composite with two so-called extraframework oxygen atoms removed.⁴¹ Hydride doping was investigated by adding one H⁻ ion (structure [Ca₂₄Al₂₈O₆₄H]³⁺ (3e⁻), abbreviated **H1**) or two H⁻ ions (structure [Ca₂₄Al₂₈O₆₄H₂]²⁺ (2e⁻), abbreviated **H2**) in the position of the extraframework oxygen atoms of the C12A7:O²⁻ mayenite oxide structure, as shown in Figure S1. The hydride ions are modeled in DFT calculations by placing hydrogen atoms inside a neutral C12A7:e⁻ cage, resulting in a formal charge of -1 that is *de facto* defined by the overall charge of the system.⁴¹ Convergence of stationary points was determined by applying a 0.05 eV/Å threshold value. The Brillouin zone was sampled by a 2 × 2 × 2 Monkhorst-Pack k-point mesh. For the hydrogen diffusion calculations in the **H1** compound, we employed the climbing-image nudged elastic band (CINEB) method implemented in VASP.⁴² The OCLIMAX software package was used to convert the DFT-predicted phonon energies into simulated INS spectra.⁴³ The simulation of phonons and the INS spectra was performed using an energy cutoff of 800 eV and a lower energy threshold of 10⁻⁸ eV for determining convergence of the wave function.

Ammonia synthesis over 2 wt % Ru/C12A7:e⁻ was carried out in a 6.4 mm outer-diameter, quartz, down-flow packed-bed reactor under differential reaction conditions. Mixtures of the feed gases H₂ (UHP, Airgas), 1% Ar in balance N₂ (certified mixture, Airgas), and He (UHP, Airgas) were introduced to the reactor through an OMI-2 gas

purifier tube (Supelco) upstream of the heated reactor bed. A loading of 15 mg of catalyst was mixed with 30 mg of 60–80 mesh quartz sand and supported on a plug of glass wool to retain the catalyst bed in the heated zone of the reactor. The products were measured at the outlet of the reactor using an onstream mass spectrometer (MS, Pfeiffer OmniStar GSD 320, 1–300 u), and all stainless-steel lines leading to the MS were heated to 423 K to reduce product readsorption in the lines. Reactants and products were monitored during each experiment by following *m/z* = 2, 4, 16, 17, 18, 28, 32, and 40, representing H₂ (*m/z* = 2), He (*m/z* = 4), NH₂/NH₃ (*m/z* = 16, 17), H₂O (*m/z* = 18), N₂ (*m/z* = 28), O₂ (*m/z* = 32), and Ar (*m/z* = 40). The quantity of NH₃ (*m/z* = 17) in the outlet was calibrated relative to Ar (*m/z* = 40) using a blend of 0.5% ammonia in N₂ (certified mixture, Airgas). Background contributions from splitting of H₂O to the NH₃ signal were removed by analyzing the cracking pattern of water vapor and correcting for the contribution to the *m/z* = 17 signal using the *m/z* = 18 signal.

Steady state, isotopic transient kinetic analysis was performed by switching between two streams of either ¹⁴N₂ (1% Ar in N₂, described above, for use as an inert tracer and internal standard) or ¹⁵N₂ (Sigma-Aldrich, 99%, 98% ¹⁵N), which are mixed on-stream with H₂ and He. The system used to acquire the transient responses has been described previously by Polo-Garzon et al.,⁴⁴ but configuration of the gas inlets and MS transfer line position were modified to reproduce the setup described by McClaine and Davis⁴⁵ where an additional gas inlet was added downstream of the 4-way valve to blend H₂ (as a reactant) or He (as a diluent) as needed into the stream of isotopically labeled or unlabeled N₂. Between 20 and 60 mg of catalyst (2 wt % of Ru supported on C12A7:e⁻ or C12A7:O²⁻) was diluted in twice the catalyst mass of 60–80 mesh quartz sand and supported on a bed of glass wool inside the quartz reactor tube. The MS transfer line was positioned as close to the end of the reactor bed as possible, to minimize any possible holdup of the products in the reactor. Conversion was kept below 30% of the equilibrium conversion to limit scrambling of ¹⁴N₂ and ¹⁵N₂. All masses monitored during steady-state experiments were also monitored here, as were *m/z* = 20 (ND₃), 29 (¹⁴N¹⁵N), and 30 (¹⁵N₂). As observed previously by McClaine et al.⁴⁵ and Siporin et al.,⁴⁶ a characteristic holdup of ammonia was observed in the reactor when switching from a stream of dilute ammonia in N₂ to pure N₂ in a reactor containing only glass wool, which was used to correct the obtained transient responses (Figure S2). All reactant and diluent gases were flowed through OMI-2 purifier tubes upstream of the reactor bed.

Temperature-programmed desorption (TPD) of D₂ (99.9%, 99.8% D, Cambridge Isotope Laboratories) and H₂ was performed using the same reactor as that used to collect the isotopic transient responses. Prior to an experiment, 50 mg of 2 wt % Ru/C12A7:e⁻ was loaded into the reactor, which was then heated to 673 K at 10 K min⁻¹ in 30 cm³ min⁻¹ of a 3:1 H₂:N₂ or D₂:N₂ gas mixture (with 1% Ar as an internal standard), held for 1 h, and then cooled to room temperature under the same environment. Once at room temperature, the reactor was purged with Ar (UHP, Airgas). The reactor was then heated back to 673 K at 10 K min⁻¹ and was held at 673 K for 1 h. Signals at *m/z* = 2 (H₂), 3 (HD), 4 (D₂), 18 (H₂O), and 20 (D₂O) were monitored throughout the experiment. Temperature-programmed surface reaction (TPSR) was carried out by first heating 50 mg of 2 wt % Ru/C12A7:e⁻ to 673 K at 10 K min⁻¹ in 30 cm³ min⁻¹ of a mixture of 3:1 D₂:N₂ and allowing ND₃ synthesis to come to a steady state over 1 h. The reactor was then cooled to room temperature, and the D₂ gas stream was switched to H₂. The reactor was then heated back to 673 K at 10 K min⁻¹ in in 75% H₂ and 25% N₂ with an Ar tracer, while *m/z* 15–20 (corresponding to all forms of partially and completely deuterated ammonia) and 40 (Ar) were monitored throughout the experiment.

3. RESULTS AND DISCUSSIONS

The electride crystal structure of C12A7:e⁻ and Ru-loaded C12A7:e⁻ was confirmed by analysis of their XRD patterns. X-ray and neutron diffraction patterns corresponding to as-

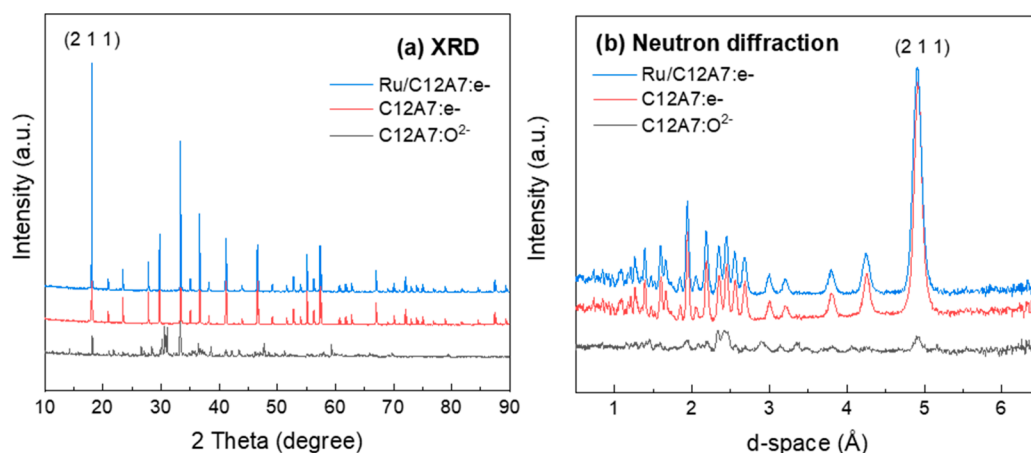


Figure 1. X-ray (a) and neutron (b) diffraction patterns obtained from C12A7:O²⁻ and C12A7:e⁻ before and after addition of Ru.

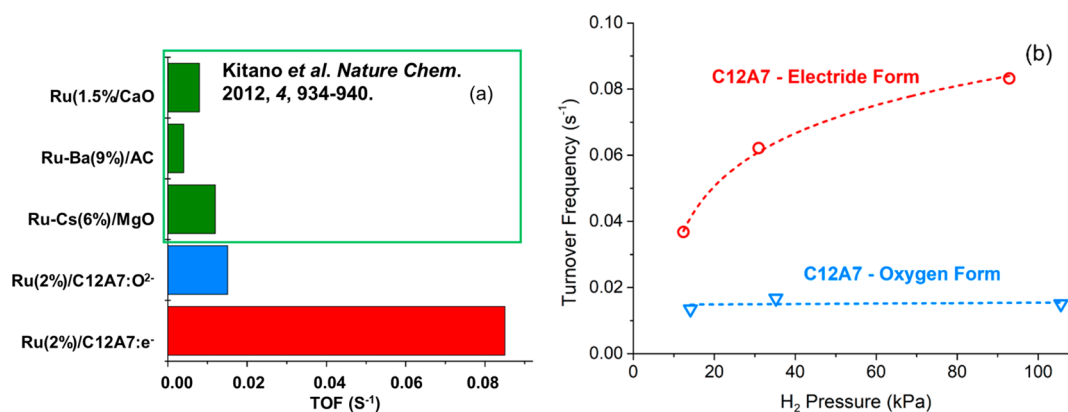


Figure 2. (a) Comparison of turnover frequency (TOF) of ammonia synthesis (normalized by CO chemisorption) at 673 K in 0.1 MPa 75% H₂ and 25% N₂ to values reported for other Ru-based catalysts in the literature.¹⁸ (b) Dependence of ammonia synthesis rate on H₂ pressure over the electride and oxygen forms of Ru/C12A7 under the same conditions.

synthesized C12A7:e⁻, Ru-loaded C12A7:e⁻, and C12A7:O²⁻ are shown in Figure 1. The composition of the stoichiometric unit cell of the electride can be expressed as [Ca₂₄Al₂₈O₆₄]⁴⁺(4e⁻). The calcium–aluminum oxide forms a positively charged three-dimensional lattice framework containing 12 cages in each unit cell. Each cage has an inner diameter of about 0.5 nm. An effective charge of +1/3 is distributed to each cage in the unit cell. Four electrons are distributed throughout the 12 cages to balance the positive charge of the framework.¹⁹ All peaks in the XRD and neutron diffraction were attributed to those of the mayenite-type crystal in the space group $I\bar{4}3d$, having a room-temperature lattice constant of 11.9 Å. Rietveld refinement from the XRD and ND revealed that after loading the Ru onto the C12A7:e⁻ the framework structure remained in agreement with the structure prior to Ru loading and thus was not degraded by the synthesis (detailed refinement results can be found in Figure S3 and Table S1 in the Supporting Information). The loading and dispersion of Ru on the C12A7 supports were verified by ICP-OES and CO chemisorption, respectively. These techniques found that Ru/C12A7:e⁻ and Ru/C12A7:O²⁻ contained 2.06 and 1.60 wt % Ru, respectively, and Ru was 5.7% and 22% dispersed on each catalyst, respectively (SEM images of Ru/C12A7:e⁻ can be found in Figure S4).

The reactivity of the electride catalyst was investigated under steady-state conditions to confirm enhanced catalytic activity for the ammonia synthesis reaction compared to other catalysts

(Figure 2). The material contained 4×10^{20} e⁻ cm⁻³ as determined by the titration method described by Yoshizumi et al.,⁴⁷ comparable to the ones reported previously for C12A7 electride.^{31,32} When loaded with 2 wt % Ru, the material catalyzed ammonia synthesis at a rate of 1.5 mmol ammonia g_{cat}⁻¹ h⁻¹ in a mixture of 75% H₂ and 25% N₂, at 633 K flowing at 30 cm³ min⁻¹. The apparent activation energy of ammonia synthesis over the material was 72 kJ mol⁻¹ (Figure S5), and ammonia synthesis was 0.7 order in N₂ pressure and 0.3 order in H₂ pressure under the conditions studied (Figure S6). Orders between 1 and 0.5 in N₂ and above zero in H₂ have been observed previously in ammonia synthesis over C12A7-electride-supported Ru, which has been thoroughly studied by Kanbara et al.⁴⁸ Normalizing the catalytic activity by the total number of Ru atoms available from CO chemisorption gave an overall turnover frequency (TOF) of 0.087 s⁻¹ over the Ru/C12A7:e⁻ in 0.1 MPa 75% H₂ and 25% N₂ at 673 K and retained its positive order in H₂ (Figure 2). For comparison, the oxygen form (no longer an electride), C12A7:O²⁻, was also tested under similar conditions for catalytic activity when loaded with 2 wt % of Ru. The TOF of ammonia synthesis was 0.015 s⁻¹, one-sixth that of the electride-supported Ru, and was zero order in H₂.¹⁹ While the dispersion of the Ru in the catalysts reported here is greater than the dispersion of Ru on C12A7 oxide forms reported elsewhere,¹⁸ the results reported here are consistent with a lack of electride promotion as demonstrated by Hara et al.¹⁹ Evidently, the electride character

Table 1. Kinetic Parameters Obtained from SSITKA during Ammonia Synthesis at 673 K Utilizing a Switch Between $^{14}\text{N}_2$ and $^{15}\text{N}_2$ ^a

catalyst	H ₂ pressure (kPa)	NH ₃ pressure (kPa)	TOF ^b (s ⁻¹)	τ_{NH_3} (s)	TOF ₀ ^c (s ⁻¹)	θ_{NH_x}
Ru/C12A7:O ²⁻	110	0.062	0.015	17.0 ± 0.7	0.060	0.095
Ru/C12A7:O ²⁻	35	0.069	0.017	24.0 ± 1.8	0.042	0.160
Ru/C12A7:O ²⁻	14	0.056	0.014	21.0 ± 0.6	0.047	0.110
Ru/C12A7:e ⁻	93	0.110	0.087	9.9 ± 2.3	0.100	0.840
Ru/C12A7:e ⁻	31	0.084	0.065	11.0 ± 0.9	0.088	0.740
Ru/C12A7:e ⁻	12	0.050	0.038	12.0 ± 1.6	0.085	0.450

^aExperiments were carried out in 0.1 MPa total pressure flowing in a mixture of H₂, 1% Ar in $^{14}\text{N}_2$ or pure $^{15}\text{N}_2$, and He at 30 cm³ min⁻¹.

^bDetermined using observed ammonia formation rate normalized by CO chemisorption. ^cIntrinsic TOF, determined from SSITKA by inverting τ_{NH_3} .

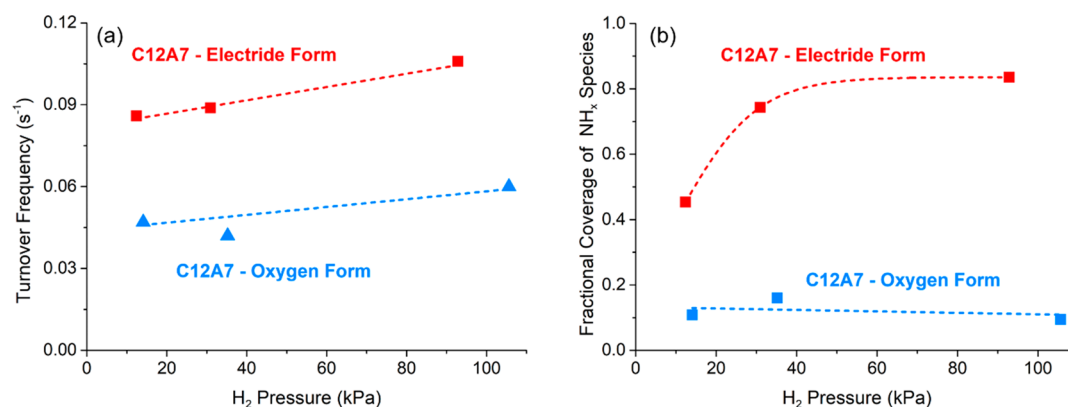


Figure 3. Intrinsic turnover frequencies (TOFs) (a) and coverages of reactive intermediates leading to ammonia (b) on the surface of 2 wt % of Ru supported on the electride or oxygen form of C12A7. Dashed lines indicate observed trends.

of the synthesized C12A7:e⁻ greatly enhanced the ammonia synthesis activity over other traditional supported Ru catalysts¹⁸ as shown in Figure 2.

Steady-state isotopic transient kinetic analysis (SSITKA) of isotopically labeled N₂ was used to determine the number of reactive N-containing intermediates present on the surface of the catalyst under reaction conditions and the intrinsic turnover frequency of N₂ incorporation into the catalytic cycle under steady-state conditions. Results of these experiments are summarized in Table 1. The exact values obtained from integration can be found in Table S2 and Figure S7. Modification of Ru-based ammonia synthesis catalysts by alkali promoters often results in an increase in ammonia synthesis rates per mass of catalyst, often proportionally to the basicity of the alkali promoter.^{49,50} The reason for this behavior can be explained by back-donation of electrons from the basic-metal-promoted active site to the antibonding π orbitals of an adsorbed N₂ molecule, which helps break the strong N \equiv N bond.⁵¹ Previous study of basic metal-promoted Ru supported on MgO showed that coverage of the Ru surface by N-containing intermediates under steady-state conditions was less than 14% under a total pressure of 3 bar, containing up to 75% H₂ and 25% N₂.

In the present study, Ru supported on C12A7:O²⁻ displayed a nearly zero-order rate and global turnover frequency dependence on H₂ pressure (Figure 2(b)). Total coverage of N-containing species on the catalyst surface was around 15% of the total Ru surface atoms measured by CO chemisorption regardless of H₂ pressure (Figure 3(b)). Results SSITKA of ammonia synthesis over similarly active Ru/MgO catalysts indicated that H₂ poisoning increased with increasing promoter basicity and suggested alkali promoters may also

increase the strength of H binding at the active sites for N₂ dissociation.⁴⁶ In contrast, the total coverage of N-containing intermediates on the Ru/C12A7:e⁻ surface reached a maximum of 84% of the total amount of surface Ru measured by CO chemisorption and decreased with decreasing H₂ pressure. It is important to note that while the results here are discussed in terms of coverage of the number of exposed Ru atoms, which are expected to be the active sites for ammonia synthesis, there may be contributions to this coverage that arise from non-Ru sites as well. While the measured SSITKA TOF increased slightly with H₂ pressure (Figure 3(a)), the total number of N-containing reactive intermediates calculated nearly doubled when H₂ pressure was increased from 12 to 93 kPa (Figure 3(b)), suggesting that the increasing H₂ pressure resulted in a higher coverage of N-containing reactive intermediates, leading to ammonia formation on the catalyst surface.

There is some debate over the reason why electron-donating promoters enhance ammonia synthesis rates over Ru catalysts. When density functional theory (DFT) was used in a previous study to probe N₂ adsorption on Ru(0001) surfaces promoted with Na and Cs, a major component of the alkali promotion was attributed to stabilization of the transition state of dissociating N₂ by direct interaction with the promoter at the active site.⁴⁹ Others have proposed, however, that electron donation from the promoter can also result in destabilization of NH_x species, leading to an increase in the number of free sites available for N₂ dissociation and thus to a promotional effect.⁵²⁻⁵⁴ This hypothesis is also supported by the comparison of microkinetic models of ammonia synthesis catalyzed by Ru or Cs-promoted Ru.^{15,16}

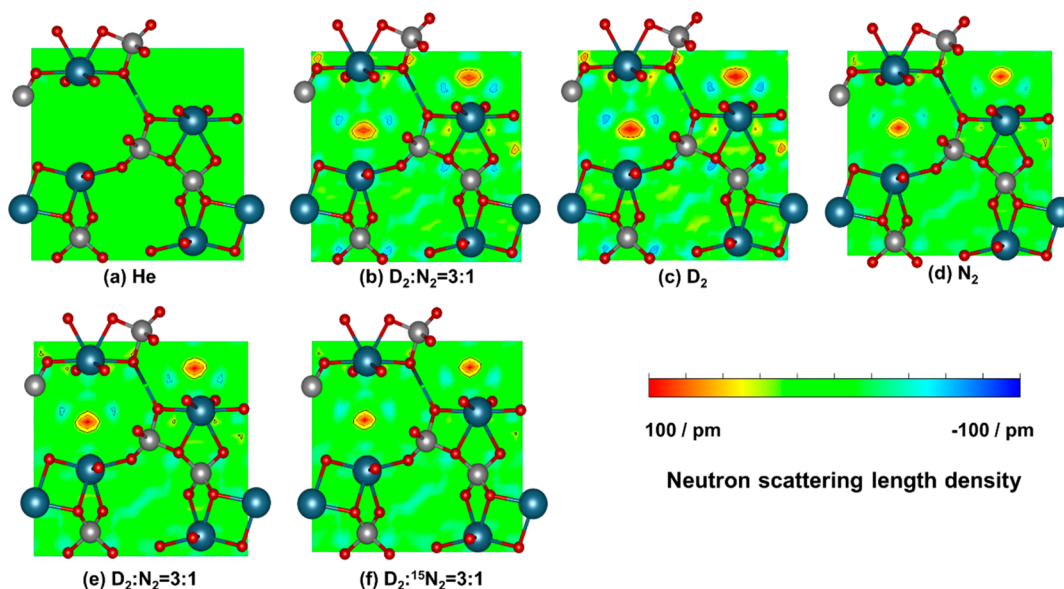


Figure 4. Difference Fourier maps created from results obtained using neutron diffraction. All maps are representations of the (001) planes in C12A7:e⁻. Diffraction patterns were obtained at 673 K after continuous reaction under conditions in the order (a) to (f) in 0.1 MPa gas pressure: (a) He treatment for 30 min, (b) D₂:N₂ = 3:1 for 3 h, (c) D₂ for 2 h, (d) N₂ for 2 h, (e) D₂:N₂ = 3:1 for 2 h, and (f) D₂:¹⁵N₂ = 3:1 for 2 h. Note that the scale for neutron-scattering length density is the same in all maps.

Evidently, the intrinsic turnover frequency of ammonia synthesis over Ru/C12A7:e⁻ has doubled compared to Ru/C12A7:O²⁻, and yet the overall rate of ammonia synthesis over Ru/C12A7:e⁻ has increased up to 6-fold compared to Ru/C12A7:O²⁻. Thus, the promotional effect of the electrone on the rate of ammonia synthesis must not result from only a large change in the ability of the Ru to dissociate N₂. Instead, we also propose that electron donation from the electrone to Ru might destabilize NH_x species (including products like NH₃), blocking active sites for N₂ dissociation on the Ru surface, which would increase the number of free sites available for reaction. This would, in turn, increase the rate of ammonia synthesis by increasing the coverage of N-containing reactive surface intermediates (for example, N₂, N*, or NH*) in quasi-equilibrium with gas-phase reactants preceding the rate-determining step. A doubling of the SSITKA TOF of ammonia synthesis over Ru/C12A7:e⁻ compared to Ru/C12A7:O²⁻ suggests that the surface of the Ru/C12A7:e⁻ should contain around 3 times more reactive intermediates turning over to products on the electrone form than the oxygen form to account for the 6-fold increase in rate. This expected value was comparable to the 5- to 6-fold increase in coverage of reactive intermediates from 15% to up to 84% observed on the Ru/C12A7:e⁻.

A fractional coverage of reactive intermediates up to 84% over Ru/C12A7:e⁻ is significantly higher than the maximum of 14% of the exposed Ru atoms observed in a previous SSITKA study of ammonia synthesis over oxide-supported Ru.⁴⁶ The increased coverage of the surface of the catalyst by N-containing reactive intermediates leading to products suggests a shift in the distribution of surface species on Ru particles in the electrone system and may even indicate a shift away from N₂ dissociation as the rate-determining step, as has been proposed elsewhere.³⁰ This might be caused by an increase in the TOF of N₂ dissociation or by freeing up enough surface sites to more than meet the demand for surface N by other active sites. If N₂ dissociation rates reach this critical level, cage hydride species would not need to play a significant role in

reactivity to mitigate the previously observed H₂ poisoning effect, as surface coverage of N-containing reactive intermediates would no longer be kinetically limited by competition between adsorbed H and N₂.

Increases in coverage of reactive intermediates arising from increased H₂ pressure suggest that the surface of the Ru/C12A7:e⁻ may be covered predominantly by a quasi-equilibrated intermediate NH_x species such as NH. Rate-determining H-addition to adsorbed NH species has been previously reported to be a candidate rate-determining step in the formation of ammonia over electrone-supported Ru particles¹⁹ and was also predicted to be the most abundant reactive intermediate on Fe and Ru surfaces during ammonia synthesis.^{8,15,30} If dissociation of adsorbed N₂ no longer dominates the rate expression, and a strongly bound surface species such as NH⁵⁴ may reach a quasi-equilibrium with gas-phase H₂ and N₂, a poisoning effect of the reactive surface by H₂ might no longer be expected. Such high coverages may also result from increased readsorption of ammonia or retention of increased amounts of NH₂ on the catalyst surface, but this hypothesis conflicts with the previously discussed expectation that destabilization of NH_x will take place when electron density is donated to the reactive surface.⁵²⁻⁵⁴

Following isotopically labeled nitrogen through the ammonia synthesis reaction cycle provides only a partial picture of the mechanism of ammonia synthesis over electrone-supported Ru. Thus, neutron-scattering techniques were applied to better understand the behavior of hydrogen-containing (and deuterium-containing) species during ammonia synthesis catalyzed by Ru/C12A7:e⁻. *In situ* neutron diffraction (ND) measurements were conducted to investigate Ru-loaded C12A7:e⁻ under several sample environments, including He, D₂:N₂ = 3:1, pure D₂, pure N₂, and D₂:¹⁵N₂ = 3:1, as described in the experimental methods. The diffraction pattern of the material during each reaction step was collected, and Rietveld refinement was conducted on the resulting diffraction pattern (Table S3). Rietveld refinement was conducted using only the framework atoms including

anisotropic atomic displacement parameters (ADPs) in order to reveal the location of the species engaged in the C12A7:e⁻ lattice using a difference Fourier map, as illustrated in Figure 4. The difference Fourier map from neutron diffraction can be used to determine the location of unidentified atoms in the structure when combined with Rietveld refinement. This technique has been used in studying the anion-loaded C12A7 structure previously to understand the mobility of extra-framework ions.^{55–57} In this case, it was possible to identify the existence of hydrogen or nitrogen in the electride framework using the obtained difference map.

An isolated atomic species in the center of the cage was observed in the Ru/C12A7:e⁻ lattice during the D₂/N₂ reaction (Figure 4b) when the measured neutron scattering density obtained from the Rietveld refinement was compared to that of the Ru/C12A7:e⁻ under He prior to the reaction (Figure 4a). The measured neutron-scattering length density from this additional atom is 65 pm, which is close to the expected scattering length density of D (66.7 pm).⁵⁸ The intensity of this feature increased slightly when the sample was exposed to D₂ (Figure 4c), but it remains stable over all the applied reaction conditions after its initial appearance (Figure 4b–f). This result suggests that the formed engaged species is very stable at 673 K. While the diffraction patterns were collected, the reactor outlet gas was analyzed using a residual gas analyzer (RGA). Using the RGA, the formation of ND₃ and ¹⁵ND₃ was confirmed during each D₂/N₂ reaction and D₂/¹⁵N₂ reaction by the presence of *m/z* = 20 and 21, respectively (Figure S8), indicating the catalyst is active for ammonia synthesis under the conditions during the ND measurements.

Based on the results from neutron diffraction, the engaged species is stable during exposure to various H₂- and N₂-containing gas-phase environments. The difference in neutron-scattering length density, however, between D (66.7 pm), ¹⁵N (64.4 pm), or O (58.0 pm)⁵⁸ is small, and thus it is hard to distinguish the identity of the unknown species in the C12A7:e⁻ cages using only their refined diffraction patterns. Because the neutron-scattering cross section is much greater for hydrogen (80 barn) than for any other element (~5 barn), displacements involving hydrogen dominate in inelastic neutron-scattering (INS) spectroscopy, and thus INS is ideal for the study of hydrogen species involved in catalytic reactions as demonstrated previously.^{59,60} To identify the cage species, *in situ* INS spectra of the Ru-loaded C12A7:e⁻ were recorded after reaction in H₂/N₂, evacuation at elevated temperature, H₂ treatment, and N₂ treatment at 673 and 873 K as described in the Materials and Methods and shown in Figures 5 and 6.

The INS spectrum of Ru/C12A7:e⁻ collected at 5 K after treatment with 0.1 MPa 3:1 H₂:N₂ at 673 K is shown in Figure 5a. The spectra shown in Figure 5 are difference spectra created by subtracting the background spectrum obtained from Ru/C12A7:e⁻ before the reaction from the spectra collected after each treatment step. After exposure of Ru/C12A7:e⁻ to the aforementioned ammonia synthesis conditions, several peaks appeared at 367, 497, 540, 622, and 728 cm⁻¹. The INS spectra of engaged hydride (simulated) and ammonia (measured) were compared to the experimentally collected spectra in Figure 5. The engaged hydride C12A7:H⁻ spectrum was predicted using DFT calculations for the conventional hydride structure containing two hydrogen atoms and two solvated electrons in the unit cell (structure [Ca₂₄Al₂₈O₆₄H₂]²⁺(2e⁻), abbreviated C12A7:H⁻) (see structure H2, Figure S1).

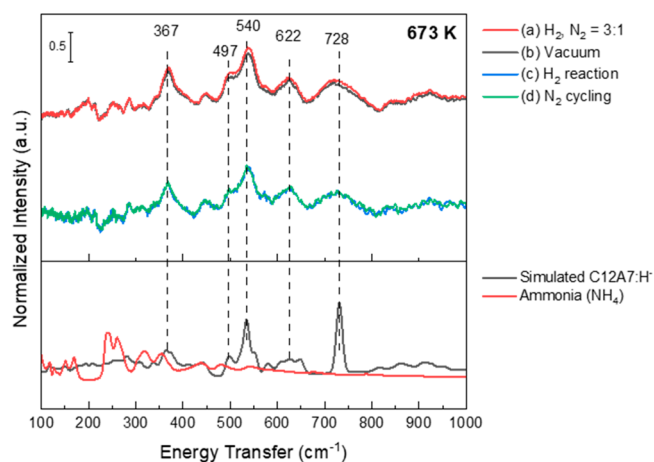


Figure 5. INS spectra of Ru/C12A7:e⁻ collected at 5 K after exposure to (a) 0.1 MPa 3:1 H₂:N₂ mixture, (b) vacuum, (c) 0.1 MPa H₂, and (d) 5 cycles of 0.1 MPa N₂ at 673 K. Spectra are offset for clarity. Simulated C12A7:H⁻ spectra and measured ammonia spectra are also shown for comparison.

The strong features observed in the experimental spectrum are markedly different than those seen in ammonia (bottom of Figure 5). They are, however, in very good agreement with the DFT-predicted features of the INS spectrum of C12A7:H⁻. The features identified by dashed lines in Figure 5 correspond to hydrogen vibrations along various axes inside the cage. The lower-frequency modes correspond to vibrations of the hydride perpendicular to the Ca–H bond (i.e., Ca–H bending), whereas the higher-frequency modes correspond to vibrations of the hydride along the Ca–H bond direction (i.e., Ca–H stretching). We suggest that the observed features arise from hydride anions in the C12A7:e⁻ lattice cages, whose location was confirmed in the above neutron diffraction experiments (Figure 4). This is, for the first time, unambiguous identification of the formation of cage hydride species in Ru/C12A7:e⁻ during ammonia synthesis.

After confirmation of the formation of engaged hydride under ammonia synthesis conditions, the sample was evacuated for 4 h at 673 K to ascertain its thermal stability (Figure 5b). The overall signal intensity from the hydride species decreased slightly after exposure to vacuum at 673 K, but evidently the majority of the hydride species remained in the C12A7:e⁻ cages. To understand the chemical stability of the hydride species, a separate experiment was conducted using a fresh sample. After heating the Ru/C12A7:e⁻ sample to 673 K, the sample container was filled with 0.1 MPa H₂ for 2 h (Figure 5c), followed by N₂ cycling (20 min in 0.1 MPa N₂ followed by evacuation, 5 cycles) (Figure 5d). The formation of engaged hydride species was confirmed after the hydrogen treatment. The intensity of hydride features observed using INS was similar after both H₂ and H₂/N₂ exposures were performed during 673 K experiments (Figure S9). After 5 cycles of N₂ exposure and evacuation, the intensity of the engaged hydride modes did not change significantly when compared to the spectrum obtained after extended exposure of the sample to H₂. This result also suggests the hydride species located in the center of the C12A7:e⁻ cages is chemically very stable. We therefore propose this hydride species is unlikely to play a significant role in the ammonia synthesis reaction.

Hayashi et al.⁶¹ reported that engaged hydride species can be released from the C12A7:e⁻ lattice as H₂ at temperatures

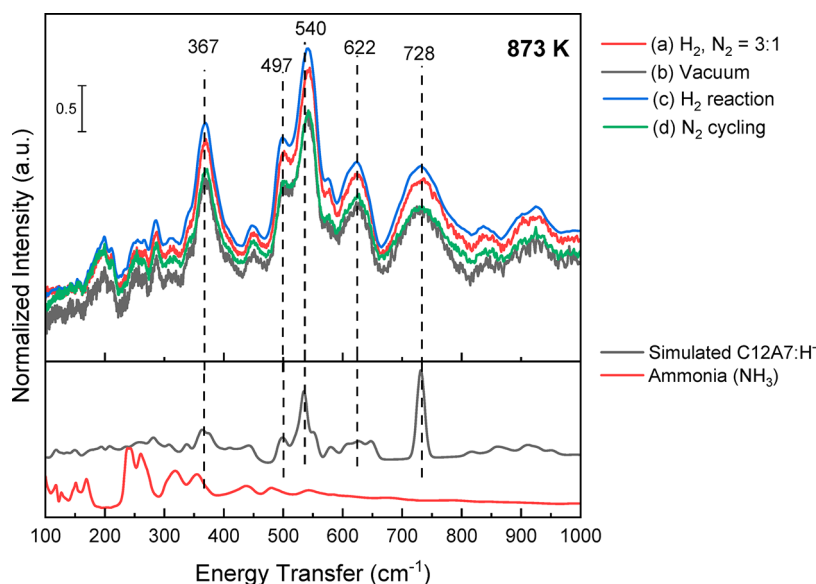


Figure 6. INS spectra of Ru/C12A7:e⁻ collected at 5 K after exposure to a (a) 0.1 MPa 3:1 H₂:N₂ mixture, (b) vacuum, (c) 0.1 MPa H₂, and (d) 5 cycles of 0.1 MPa N₂ at 873 K. Simulated C12A7:H⁻ spectra and measured ammonia spectra are also shown for comparison at the bottom of the figure. Note that these experiments were conducted after the experiments shown in Figure 5a and b.

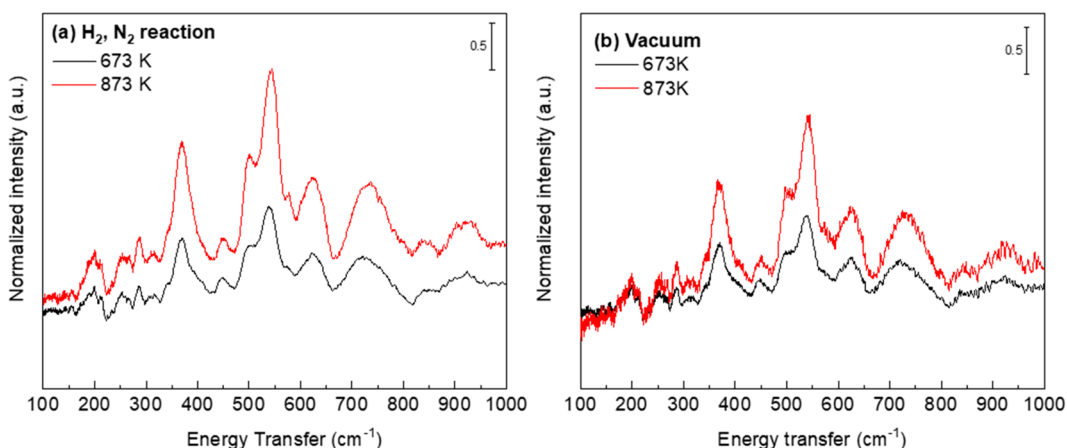


Figure 7. Comparison between INS spectra collected after treatment at 673 and 873 K in (a) 3:1 H₂:N₂ ammonia synthesis conditions and (b) vacuum.

above 873 K, so the behavior of the engaged hydride species was also investigated at this temperature using INS. After the evacuation experiment at 673 K, the reaction temperature was increased to 873 K, and the sample was again exposed to a 3:1 mixture of H₂ and N₂. The intensity of the INS spectrum after exposure to the H₂/N₂ mixture at 873 K was nearly twice that of the spectrum collected after exposure to the same environment at 673 K (Figures 6a and 7a). This indicates that under typical ammonia synthesis temperatures (673 K or lower) over Ru/C12A7:e⁻ the support electrons are only partially replaced by hydrides and thus can still impact the reaction. After evacuation at 873 K for 4 h, the intensity of the hydride features decreased significantly (Figures 6b and 7b) but was still of a higher intensity than that of the sample after exposure to H₂/N₂ followed by evacuation at 673 K. To understand the reactivity of the cage hydride at 873 K, the sample was exposed to 0.1 MPa H₂ to reform the hydride, which was followed (after evacuation, cooling, and measurement) by N₂ cycling. After H₂ treatment (Figure 6c), the intensity of the INS features associated with engaged hydride

species was slightly higher than that observed after the H₂/N₂ reaction (Figure 6a). After N₂ cycling (Figure 6d), the intensity of the engaged hydride signal formed during H₂ exposure decreased by 40%, to a similar intensity as that observed after evacuation (Figure 6b, black trace) at 873 K. Compared to results obtained at 673 K, this decrease suggests that more hydride species can be incorporated into the electrode cage at a higher temperature but that the hydrides incorporated at high temperature are less stable at the elevated temperature (possibly indicating engaged hydride located deeper in the bulk of the material). Because the intensity of the INS features associated with hydride species in the Ru/C12A7:e⁻ cages after ammonia synthesis/evacuation for 4 h and after H₂ exposure/N₂ cycling (Figure 6b and d, respectively) was so similar, the decrease in intensity in the hydride features after N₂ cycling was likely a result of thermal desorption of those species. Closer analysis found a gradual decrease of the engaged hydride features after each N₂ cycle, indicating a slow removal process (Figure S10).

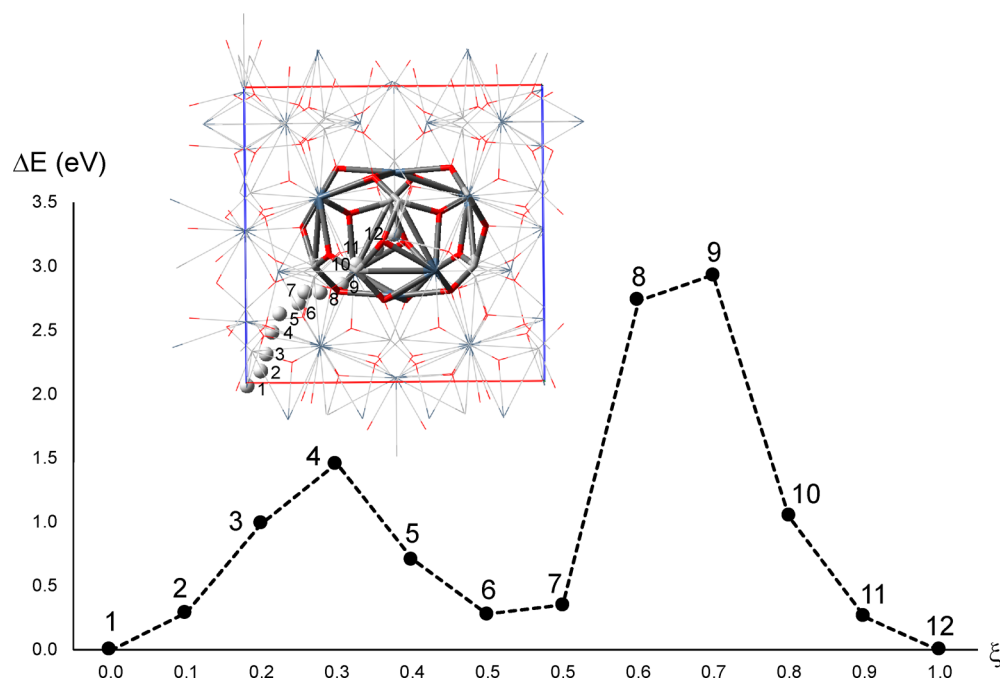


Figure 8. PAW-PBE-optimized minimum energy pathway of a hydrogen atom from position 1 to position 12, connecting the two energy-equivalent positions. ξ represents the reaction coordinate, and ΔE measures the height of the isomer positions from the minimum energy structures in 1 and 12.

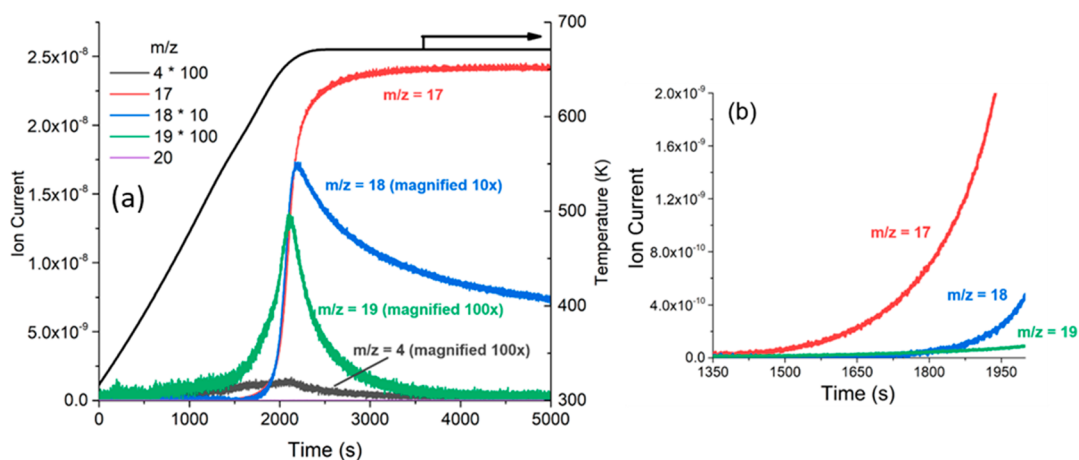


Figure 9. (a) Temperature-programmed surface reaction ion current traces and temperature profile during ammonia synthesis in 75% H_2 and 25% N_2 after exposure to 75% D_2 and 25% N_2 at 673 K for 1 h. (b) Close-up view (not magnified) of the onset of ammonia production during the TPSR experiment.

To understand the difficulty of removing hydride species from C12A7:e^- cages, the energetic barriers for the diffusion of hydride between cages were calculated using DFT. These hydrides are predicted to be bound in the center of the electrified cages with high binding energy, using neutral hydrogen atoms and the C12A7:e^- as a reference; we determined them to be 3.2 eV in the case of the open-shell radical **H1** and 8.2 eV in the case of the closed-shell **H2** hydride compound (Figure S1). Evidently, the adsorption of two hydride ions in the unit cell is preferable to the adsorption of two hydrogens in two isolated unit cells, due to the delocalized nature of the electronic states. To determine how easily hydride ions can diffuse into and through the bulk, we modeled the ion migration in structure **H1** from one of the symmetry-equivalent hydride ion positions to the other in compound **H2**, as shown in Figure 8. Interestingly, we found

that the energetically most favorable pathway for the hydride diffusion from one cage to a neighboring cage involves an intermediate minimum-energy structure at point 6 of the potential energy curve, where the hydride ion is closely bound to cage Ca atoms with a bond distance of 2.3–2.5 Å. The diffusion barrier for hydride migration from position **H1** to the intermediate position (point 6, Figure 8) is predicted to be ~ 1.5 eV, whereas a larger barrier of around 2.9 eV is predicted for the entrance of the hydrogen into the central cage to reach position 12, equivalent to the second hydride position in compound **H2**. The reason for the two barriers and their different energy values lies in the fact that the cages have local S_4 symmetry with an asymmetric intermediate minimum, allowing two different, but symmetry-equivalent, pathways connecting the three stationary points. No energetically more favorable pathways for hydride diffusion between a cage wall

and the center of the cage were identified, which agrees with our observation that hydrogen can enter the electronegative only at high temperatures. While H^- may be capable of tunneling through these high barriers at some appreciable rate,⁶² the barrier to H_2 dissociation on the Ru surface (which is traditionally believed to contain the active site for ammonia synthesis) is often considered negligible,¹⁶ and thus the supply of reactive H to an active site on Ru is likely to come directly from a nearby site on the Ru surface.

As neutron scattering and DFT suggested cage hydride species are stable and unlikely to be reactive under ammonia synthesis conditions, temperature-programmed desorption and surface reaction (TPD and TPSR) were used to characterize the observable reactivity of encaged hydride species. The TPR and TPSR experiments were carried out using Ru/C12A7:e⁻ after exposure to ND_3 synthesis conditions (75% D_2 , 25% Ar/N_2) for 1 h, and following cooling to room temperature in the same gas composition resulted in the background-subtracted mass traces shown in Figure S11. Results from the TPD indicated that only a small fraction of encaged D, about $5 \mu\text{mol g}^{-1}$, could be removed in the forms of HD and D_2 from the Ru/C12A7:e⁻ when the catalyst was heated to 673 K in an Ar atmosphere. The appearance of H in the product (HD) is likely from the background water in the system. This quantity of $\sim 5 \mu\text{mol g}^{-1}$ was equal to only 50% of the available Ru surface determined by CO chemisorption and is therefore not distinguishable from D species located entirely on the Ru surface. When a similarly treated catalyst was heated to 673 K in a 75% H_2 and 25% N_2 atmosphere, nearly 18 times more D was observed ($95 \mu\text{mol g}^{-1}$) in the outlet stream in the form of ND_x ($x = 1-2$) and D_2 during the temperature-programmed experiment (Figure 9). This quantity represented 800% of the total number of available Ru surface atoms determined from CO chemisorption, indicating likely incorporation of encaged D species into the reaction cycle. This indicated that encaged D species are stable in the electronegative cages even to 673 K and that encaged H/D species were more effectively removed under ammonia synthesis conditions, where the species are either reacting with N or being displaced by exchange with the gas-phase H_2 .

Evidently, the surface reaction between gas-phase N_2 and H_2 occurred faster than the reaction between encaged D species and adsorbed N species. When deuterium incorporation into product ammonia during the TPSR was investigated, production of deuterated species was not observed until after the formation of completely unlabeled products (Figure 9b). Completely deuterated ammonia ($m/z = 20$) was not observed, and the predominantly observed species was nondeuterated ammonia, with singly deuterated product (NDH_2) reaching a maximum of 12% of the observed products, suggesting that most encaged species are not participating directly in product formation but may still be capable of exchanging with H or D species already on the catalytically active surface. As earlier results from neutron scattering and density functional theory indicated that encaged hydrides are very stable in the electronegative cages, with theoretical barriers to diffusion much higher than those observed for the rate of ammonia synthesis, their participation in the reaction is unlikely. While it is evident that a fraction of encaged species is exchanging with the reactive surface H_2 , there is not enough evidence to suggest that the presence of these species contributes significantly to the synthesis of ammonia, especially if those encaged species are not contained in a cage that

borders the surface interface. Instead, we propose that surface-adsorbed H and D species contribute to the vast majority of catalytic ammonia synthesis activity in C12A7:e⁻-supported Ru catalysts, and the active site for catalysis is on the Ru surface in this system. Two-dimensional electrides, which emerged recently in both experimental and computational work,⁶³⁻⁶⁵ may provide a new revenue to utilize the formed hydride species under ammonia reaction conditions due to the reduced bulk dimension and thus possibly reduced barriers for hydride diffusion.

4. CONCLUSIONS

We have demonstrated for the first time the presence of hydride species in the framework of Ru/C12A7 electronegative using *in situ* neutron-scattering techniques. Results from neutron diffraction, INS, DFT, and temperature-programmed reduction and surface reaction experiments suggested that the encaged hydrides are stable in the C12A7:e⁻ cages and do not exchange readily on their own or incorporate into the product ammonia. While these species could exchange with other surface species, they appear unlikely to be playing a major kinetic role in the mechanism of ammonia synthesis. Instead, hydrogen species adsorbed on the Ru surface predominantly participate in ammonia synthesis. Using steady-state transient kinetic analysis, coverages of reactive intermediates on the Ru/C12A7:e⁻ of up to 84% of the number of exposed Ru surface atoms (as determined by CO chemisorption) were observed, which was 5 to 6 times higher than the coverage observed on the Ru/C12A7:O²⁻. These results indicated that a major shift in the coverage of reactive intermediates on the catalyst surface takes place when the Ru surface is promoted by an electronegative support. Indeed, this change in the makeup of adsorbates on the Ru surface is likely to be the reason that H_2 poisoning effects are not observed during ammonia synthesis catalyzed by the electronegative-supported Ru. The finding from this work sheds new insights into the reaction mechanism of ammonia synthesis over electronegative-based catalysts.

■ ASSOCIATED CONTENT

SI Supporting Information

The Supporting Information is available free of charge at <https://pubs.acs.org/doi/10.1021/jacs.0c02345>.

Optimized C12A7:e⁻ hydride structures, calibration and supporting SSITKA results, Rietveld refinement results, apparent activation energy and orders of reaction of ammonia synthesis over Ru/C12A7:e⁻, residual gas analysis obtained during neutron diffraction experiments, inelastic neutron scattering results, temperature-programmed desorption curves, and Cartesian coordinates of optimized structures (PDF)

■ AUTHOR INFORMATION

Corresponding Author

Zili Wu – Chemical Sciences Division and Center for Nanophase Materials Sciences, Oak Ridge National Laboratory, Oak Ridge, Tennessee 37831, United States; orcid.org/0000-0002-4468-3240; Email: wuz1@ornl.gov

Authors

James Kammert – Chemical Sciences Division, Oak Ridge National Laboratory, Oak Ridge, Tennessee 37831, United States

Jisue Moon – Chemical Sciences Division and Center for Nanophase Materials Sciences, Oak Ridge National Laboratory, Oak Ridge, Tennessee 37831, United States

Yongqiang Cheng – Neutron Scattering Division, Oak Ridge National Laboratory, Oak Ridge, Tennessee 37831, United States; orcid.org/0000-0002-3263-4812

Luke Daemen – Neutron Scattering Division, Oak Ridge National Laboratory, Oak Ridge, Tennessee 37831, United States

Stephan Irlé – Chemical Sciences Division, Oak Ridge National Laboratory, Oak Ridge, Tennessee 37831, United States; orcid.org/0000-0003-4995-4991

Victor Fung – Center for Nanophase Materials Sciences, Oak Ridge National Laboratory, Oak Ridge, Tennessee 37831, United States; orcid.org/0000-0002-3347-6983

Jue Liu – Neutron Scattering Division, Oak Ridge National Laboratory, Oak Ridge, Tennessee 37831, United States; orcid.org/0000-0002-4453-910X

Katharine Page – Neutron Scattering Division, Oak Ridge National Laboratory, Oak Ridge, Tennessee 37831, United States; orcid.org/0000-0002-9071-3383

Xiaohan Ma – Center for Nanophase Materials Sciences, Oak Ridge National Laboratory, Oak Ridge, Tennessee 37831, United States; Department of Materials Science and Engineering, Clemson University, Clemson, South Carolina 29634, United States

Vincent Phaneuf – Department of Materials Science and Engineering, Clemson University, Clemson, South Carolina 29634, United States

Jianhua Tong – Department of Materials Science and Engineering, Clemson University, Clemson, South Carolina 29634, United States; orcid.org/0000-0002-0684-1658

Anibal J. Ramirez-Cuesta – Neutron Scattering Division, Oak Ridge National Laboratory, Oak Ridge, Tennessee 37831, United States

Complete contact information is available at:
<https://pubs.acs.org/10.1021/jacs.0c02345>

Author Contributions

#J.K. and J.M. contributed equally to this work

Notes

This manuscript has been authored by UT-Battelle, LLC under Contract No. DE-AC05-00OR22725 with the U.S. Department of Energy. The United States Government retains and the publisher, by accepting the article for publication, acknowledges that the United States Government retains a nonexclusive, paid-up, irrevocable, worldwide license to publish or reproduce the published form of this manuscript, or allow others to do so, for United States Government purposes. The Department of Energy will provide public access to these results of federally sponsored research in accordance with the DOE Public Access Plan (<http://energy.gov/downloads/doe-public-access-plan>).

The authors declare no competing financial interest.

ACKNOWLEDGMENTS

This research is sponsored by the Laboratory Directed Research Development (LDRD) of Oak Ridge National Laboratory, managed by UT-Battelle, LLC, for the U.S. Department of Energy. The neutron studies were conducted at the Spallation Neutron Source, a DOE Office of Science User Facility operated by the Oak Ridge National Laboratory.

Part of the catalyst synthesis and SEM imaging were conducted at the Center for Nanophase Materials Sciences, a DOE Office of Science User Facility. This research used resources of the National Energy Research Scientific Computing Center, a DOE Office of Science User Facility supported by the Office of Science of the U.S. Department of Energy under contract no. DE-AC02-05CH11231, and resources of the Compute and Data Environment for Science (CADES) at the Oak Ridge National Laboratory, which is supported by the Office of Science of the U.S. Department of Energy under Contract No. DE-AC05-00OR22725. Helpful discussions with Aditya (Ashi) Savara and Felipe Polo-Garzon are acknowledged.

REFERENCES

- (1) Erisman, J. W.; Sutton, M. A.; Galloway, J.; Klimont, Z.; Winiwarter, W. How a century of ammonia synthesis changed the world. *Nat. Geosci.* **2008**, *1* (10), 636–639.
- (2) Metkemeijer, R.; Achard, P. Ammonia as a feedstock for a hydrogen fuel cell; reformer and fuel cell behaviour. *J. Power Sources* **1994**, *49* (1–3), 271–282.
- (3) Zamfirescu, C.; Dincer, I. Ammonia as a green fuel and hydrogen source for vehicular applications. *Fuel Process. Technol.* **2009**, *90* (5), 729–737.
- (4) Klerke, A.; Christensen, C. H.; Nørskov, J. K.; Vegge, T. Ammonia for hydrogen storage: challenges and opportunities. *J. Mater. Chem.* **2008**, *18* (20), 2304–2310.
- (5) Dumesic, J. A.; Topsøe, H.; Khammouma, S.; Boudart, M. Surface, catalytic and magnetic properties of small iron particles: II. Structure sensitivity of ammonia synthesis. *J. Catal.* **1975**, *37* (3), 503–512.
- (6) Strongin, D.; Carrazza, J.; Bare, S. R.; Somorjai, G. A. The importance of C7 sites and surface roughness in the ammonia synthesis reaction over iron. *J. Catal.* **1987**, *103* (1), 213–215.
- (7) Ertl, G. Primary steps in catalytic synthesis of ammonia. *J. Vac. Sci. Technol., A* **1983**, *1* (2), 1247–1253.
- (8) Boudart, M. Kinetics and Mechanism of Ammonia Synthesis. *Catal. Rev.: Sci. Eng.* **1981**, *23* (1–2), 1–15.
- (9) Saadatjou, N.; Jafari, A.; Sahebdehfar, S. Ruthenium Nanocatalysts for Ammonia Synthesis: A Review. *Chem. Eng. Commun.* **2015**, *202* (4), 420–448.
- (10) Aika, K.-i. Role of alkali promoter in ammonia synthesis over ruthenium catalysts—Effect on reaction mechanism. *Catal. Today* **2017**, *286*, 14–20.
- (11) Dahl, S.; Logadottir, A.; Egeberg, R. C.; Larsen, J. H.; Chorkendorff, I.; Törnqvist, E.; Nørskov, J. K. Role of Steps in N₂ Activation on Ru(0001). *Phys. Rev. Lett.* **1999**, *83* (9), 1814–1817.
- (12) Dahl, S.; Törnqvist, E.; Chorkendorff, I. Dissociative adsorption of N on Ru(0001): A surface reaction totally dominated by steps. *J. Catal.* **2000**, *192* (2), 381–390.
- (13) Jacobsen, C. J. H.; Dahl, S.; Hansen, P. L.; Törnqvist, E.; Jensen, L.; Topsøe, H.; Prip, D. V.; Møenshaug, P. B.; Chorkendorff, I. Structure sensitivity of supported ruthenium catalysts for ammonia synthesis. *J. Mol. Catal. A: Chem.* **2000**, *163* (1–2), 19–26.
- (14) Rosowski, F.; Hornung, A.; Hinrichsen, O.; Herein, D.; Muhler, M.; Ertl, G. Ruthenium catalysts for ammonia synthesis at high pressures: Preparation, characterization, and power-law kinetics. *Appl. Catal., A* **1997**, *151* (2), 443–460.
- (15) Dahl, S.; Sehested, J.; Jacobsen, C.; Törnqvist, E.; Chorkendorff, I. Surface science based microkinetic analysis of ammonia synthesis over ruthenium catalysts. *J. Catal.* **2000**, *192* (2), 391–399.
- (16) Hinrichsen, O.; Rosowski, F.; Muhler, M.; Ertl, G. The microkinetics of ammonia synthesis catalyzed by cesium-promoted supported ruthenium. *Chem. Eng. Sci.* **1996**, *51* (10), 1683–1690.
- (17) Matsuishi, S.; Toda, Y.; Miyakawa, M.; Hayashi, K.; Kamiya, T.; Hirano, M.; Tanaka, I.; Hosono, H. High-density electron anions in a nanoporous single crystal: [Ca₂₄Al₂₈O₆₄]^{4+(4e-)}. *Science* **2003**, *301* (5633), 626–9.

- (18) Kitano, M.; Inoue, Y.; Yamazaki, Y.; Hayashi, F.; Kanbara, S.; Matsuishi, S.; Yokoyama, T.; Kim, S. W.; Hara, M.; Hosono, H. Ammonia synthesis using a stable electrider as an electron donor and reversible hydrogen store. *Nat. Chem.* **2012**, *4* (11), 934–40.
- (19) Hara, M.; Kitano, M.; Hosono, H. Ru-Loaded C12A7:e-Electrider as a Catalyst for Ammonia Synthesis. *ACS Catal.* **2017**, *7* (4), 2313–2324.
- (20) Kitano, M.; Kanbara, S.; Inoue, Y.; Kuganathan, N.; Sushko, P. V.; Yokoyama, T.; Hara, M.; Hosono, H. Electrider support boosts nitrogen dissociation over ruthenium catalyst and shifts the bottleneck in ammonia synthesis. *Nat. Commun.* **2015**, *6* (1), 6731.
- (21) Lu, Y.; Li, J.; Tada, T.; Toda, Y.; Ueda, S.; Yokoyama, T.; Kitano, M.; Hosono, H. Water Durable Electrider Y(5)Si(3): Electronic Structure and Catalytic Activity for Ammonia Synthesis. *J. Am. Chem. Soc.* **2016**, *138* (12), 3970–3.
- (22) Wu, J.; Gong, Y.; Inoshita, T.; Fredrickson, D. C.; Wang, J.; Lu, Y.; Kitano, M.; Hosono, H. Tiered Electron Anions in Multiple Voids of LaScSi and Their Applications to Ammonia Synthesis. *Adv. Mater.* **2017**, *29* (36), 1700924.
- (23) Ogawa, T.; Kobayashi, Y.; Mizoguchi, H.; Kitano, M.; Abe, H.; Tada, T.; Toda, Y.; Niwa, Y.; Hosono, H. High Electron Density on Ru in Intermetallic YRu₂: The Application to Catalyst for Ammonia Synthesis. *J. Phys. Chem. C* **2018**, *122* (19), 10468–10475.
- (24) Kitano, M.; Inoue, Y.; Ishikawa, H.; Yamagata, K.; Nakao, T.; Tada, T.; Matsuishi, S.; Yokoyama, T.; Hara, M.; Hosono, H. Essential role of hydride ion in ruthenium-based ammonia synthesis catalysts. *Chem. Sci.* **2016**, *7* (7), 4036–4043.
- (25) Tang, Y.; Kobayashi, Y.; Masuda, N.; Uchida, Y.; Okamoto, H.; Kageyama, T.; Hosokawa, S.; Loyer, F.; Mitsuhara, K.; Yamanaka, K.; Tamenori, Y.; Tassel, C.; Yamamoto, T.; Tanaka, T.; Kageyama, H. Metal-Dependent Support Effects of Oxyhydride-Supported Ru, Fe, Co Catalysts for Ammonia Synthesis. *Adv. Energy Mater.* **2018**, *8* (36), 1801772.
- (26) Gao, W.; Guo, J.; Chen, P. Hydrides, Amides and Imides Mediated Ammonia Synthesis and Decomposition. *Chin. J. Chem.* **2019**, *37* (5), 442–451.
- (27) Wang, Q.; Guo, J.; Chen, P. Recent progress towards mild-condition ammonia synthesis. *J. Energy Chem.* **2019**, *36*, 25–36.
- (28) Wang, P.; Chang, F.; Gao, W.; Guo, J.; Wu, G.; He, T.; Chen, P. Breaking scaling relations to achieve low-temperature ammonia synthesis through LiH-mediated nitrogen transfer and hydrogenation. *Nat. Chem.* **2017**, *9* (1), 64–70.
- (29) Chang, F.; Guan, Y.; Chang, X.; Guo, J.; Wang, P.; Gao, W.; Wu, G.; Zheng, J.; Li, X.; Chen, P. Alkali and Alkaline Earth Hydrides-Driven N₂ Activation and Transformation over Mn Nitride Catalyst. *J. Am. Chem. Soc.* **2018**, *140* (44), 14799–14806.
- (30) Kobayashi, Y.; Kitano, M.; Kawamura, S.; Yokoyama, T.; Hosono, H. Kinetic evidence: the rate-determining step for ammonia synthesis over electrider-supported Ru catalysts is no longer the nitrogen dissociation step. *Catal. Sci. Technol.* **2017**, *7* (1), 47–50.
- (31) Jiang, D.; Zhao, Z.; Mu, S.; Phaneuf, V.; Tong, J. Simple and Efficient Fabrication of Mayenite Electrideres from a Solution-Derived Precursor. *Inorg. Chem.* **2017**, *56* (19), 11702–11709.
- (32) Jiang, D.; Zhao, Z.; Mu, S.; Qian, H.; Tong, J. Facile and Massive Aluminothermic Synthesis of Mayenite Electrideres from Cost-Effective Oxide and Metal Precursors. *Inorg. Chem.* **2019**, *58* (1), 960–967.
- (33) Betta, R. A. D. Measurement of ruthenium metal surface area by chemisorption. *J. Catal.* **1974**, *34* (1), 57–60.
- (34) Neufeind, J.; Feygenson, M.; Carruth, J.; Hoffmann, R.; Chipley, K. K. The Nanoscale Ordered MAterials Diffractometer NOMAD at the Spallation Neutron Source SNS. *Nucl. Instrum. Methods Phys. Res., Sect. B* **2012**, *287*, 68–75.
- (35) Toby, B. H.; Von Dreele, R. B. GSAS-II: the genesis of a modern open-source all purpose crystallography software package. *J. Appl. Crystallogr.* **2013**, *46* (2), 544–549.
- (36) Momma, K.; Izumi, F. VESTA 3 for three-dimensional visualization of crystal, volumetric and morphology data. *J. Appl. Crystallogr.* **2011**, *44* (6), 1272–1276.
- (37) Kresse, G.; Furthmüller, J. Efficient iterative schemes for ab initio total-energy calculations using a plane-wave basis set. *Phys. Rev. B: Condens. Matter Mater. Phys.* **1996**, *54* (16), 11169–11186.
- (38) Perdew, J. P.; Burke, K.; Ernzerhof, M. Generalized Gradient Approximation Made Simple. *Phys. Rev. Lett.* **1996**, *77* (18), 3865–3868.
- (39) Blöchl, P. E. Projector augmented-wave method. *Phys. Rev. B: Condens. Matter Mater. Phys.* **1994**, *50* (24), 17953–17979.
- (40) Kresse, G.; Joubert, D. From ultrasoft pseudopotentials to the projector augmented-wave method. *Phys. Rev. B: Condens. Matter Mater. Phys.* **1999**, *59* (3), 1758–1775.
- (41) Sushko, P. V.; Shluger, A. L.; Hayashi, K.; Hirano, M.; Hosono, H. Role of hydrogen atoms in the photoinduced formation of stable electron centers in H-doped 12CaO·7Al₂O₃. *Phys. Rev. B: Condens. Matter Mater. Phys.* **2006**, *73* (4), 045120.
- (42) Henkelman, G.; Uberuaga, B. P.; Jónsson, H. A climbing image nudged elastic band method for finding saddle points and minimum energy paths. *J. Chem. Phys.* **2000**, *113* (22), 9901–9904.
- (43) Cheng, Y. Q.; Daemen, L. L.; Kolesnikov, A. I.; Ramirez-Cuesta, A. J. Simulation of Inelastic Neutron Scattering Spectra Using OCLIMAX. *J. Chem. Theory Comput.* **2019**, *15* (3), 1974–1982.
- (44) Polo-Garzon, F.; Fung, V.; Nguyen, L.; Tang, Y.; Tao, F.; Cheng, Y.; Daemen, L. L.; Ramirez-Cuesta, A. J.; Foo, G. S.; Zhu, M.; Wachs, I. E.; Jiang, D. E.; Wu, Z. Elucidation of the Reaction Mechanism for High-Temperature Water Gas Shift over an Industrial-Type Copper-Chromium-Iron Oxide Catalyst. *J. Am. Chem. Soc.* **2019**, *141* (19), 7990–7999.
- (45) McClaine, B. C.; Davis, R. J. Isotopic transient kinetic analysis of Cs-promoted Ru/MgO during ammonia synthesis. *J. Catal.* **2002**, *210* (2), 387–396.
- (46) Siporin, S. E.; Davis, R. J. Isotopic transient analysis of ammonia synthesis over Ru/MgO catalysts promoted by cesium, barium, or lanthanum. *J. Catal.* **2004**, *222* (2), 315–322.
- (47) Yoshizumi, T.; Matsuishi, S.; Kim, S.-W.; Hosono, H.; Hayashi, K. Iodometric Determination of Electrons Incorporated into Cages in 12CaO·7Al₂O₃ Crystals. *J. Phys. Chem. C* **2010**, *114* (36), 15354–15357.
- (48) Kanbara, S.; Kitano, M.; Inoue, Y.; Yokoyama, T.; Hara, M.; Hosono, H. Mechanism Switching of Ammonia Synthesis Over Ru-Loaded Electrider Catalyst at Metal-Insulator Transition. *J. Am. Chem. Soc.* **2015**, *137* (45), 14517–24.
- (49) Mortensen, J. J.; Hammer, B.; Nørskov, J. K. Alkali Promotion of N₂ Dissociation over Ru(0001). *Phys. Rev. Lett.* **1998**, *80* (19), 4333–4336.
- (50) Hikita, T.; Kadowaki, Y.; Aika, K. Promoter action of alkali nitrate in Raney ruthenium catalyst for activation of dinitrogen. *J. Phys. Chem.* **1991**, *95* (23), 9396–9402.
- (51) Rao, C. N. R.; Ranga Rao, G. Nature of nitrogen adsorbed on transition metal surfaces as revealed by electron spectroscopy and cognate techniques. *Surf. Sci. Rep.* **1991**, *13* (7), 223–263.
- (52) Strongin, D.; Somorjai, G. A. The effects of potassium on ammonia synthesis over iron single-crystal surfaces. *J. Catal.* **1988**, *109* (1), 51–60.
- (53) Dahl, S.; Logadóttir, A.; Jacobsen, C. J. H.; Nørskov, J. K. Electronic factors in catalysis: the volcano curve and the effect of promotion in catalytic ammonia synthesis. *Appl. Catal., A* **2001**, *222* (1–2), 19–29.
- (54) Logadóttir, A.; Nørskov, J. K. Ammonia synthesis over a Ru(0001) surface studied by density functional calculations. *J. Catal.* **2003**, *220* (2), 273–279.
- (55) Boysen, H.; Lerch, M.; Stys, A.; Senyshyn, A. Structure and oxygen mobility in mayenite (Ca₁₂Al₁₄O₃₃): a high-temperature neutron powder diffraction study. *Acta Crystallogr., Sect. B: Struct. Sci.* **2007**, *63* (5), 675–682.
- (56) Palacios, L.; Cabeza, A.; Bruque, S.; García-Granda, S.; Aranda, M. A. G. Structure and Electrons in Mayenite Electrideres. *Inorg. Chem.* **2008**, *47* (7), 2661–2667.

(57) Hayashi, K.; Sushko, P. V.; Hashimoto, Y.; Shluger, A. L.; Hosono, H. Hydride ions in oxide hosts hidden by hydroxide ions. *Nat. Commun.* **2014**, *5* (1), 3515.

(58) Hutchings, M. T.; Withers, P. J.; Holden, T. M.; Lorentzen, T. *Introduction to the characterization of residual stress by neutron diffraction*; CRC press: 2005.

(59) Polo-Garzon, F.; Luo, S.; Cheng, Y.; Page, K. L.; Ramirez-Cuesta, A. J.; Britt, P. F.; Wu, Z. Neutron Scattering Investigations of Hydride Species in Heterogeneous Catalysis. *ChemSusChem* **2019**, *12* (1), 93–103.

(60) O'Malley, A. J.; Parker, S. F.; Catlow, C. R. A. Neutron spectroscopy as a tool in catalytic science. *Chem. Commun.* **2017**, *53* (90), 12164–12176.

(61) Hayashi, K.; Sushko, P. V.; Shluger, A. L.; Hirano, M.; Hosono, H. Hydride Ion as a Two-Electron Donor in a Nanoporous Crystalline Semiconductor $12\text{CaO}\cdot 7\text{Al}_2\text{O}_3$. *J. Phys. Chem. B* **2005**, *109* (50), 23836–23842.

(62) McMahon, R. J. Chemistry. Chemical reactions involving quantum tunneling. *Science* **2003**, *299* (5608), 833–4.

(63) Druffel, D. L.; Kuntz, K. L.; Woomer, A. H.; Alcorn, F. M.; Hu, J.; Donley, C. L.; Warren, S. C. Experimental Demonstration of an Electride as a 2D Material. *J. Am. Chem. Soc.* **2016**, *138* (49), 16089–16094.

(64) Druffel, D. L.; Woomer, A. H.; Kuntz, K. L.; Pawlik, J. T.; Warren, S. C. Electrons on the surface of 2D materials: from layered electrides to 2D electrenes. *J. Mater. Chem. C* **2017**, *5* (43), 11196–11213.

(65) Kitano, M.; Inoue, Y.; Sasase, M.; Kishida, K.; Kobayashi, Y.; Nishiyama, K.; Tada, T.; Kawamura, S.; Yokoyama, T.; Hara, M.; Hosono, H. Self-organized Ruthenium–Barium Core–Shell Nanoparticles on a Mesoporous Calcium Amide Matrix for Efficient Low-Temperature Ammonia Synthesis. *Angew. Chem., Int. Ed.* **2018**, *57* (10), 2648–2652.